

Titre: Radiotherapy immobilization mask molding through the use of 3D-printed head models

Auteurs: Quoc-Viet Vincent Pham, Annie-Pier Lavallee, Alexandru Foias, David Roberge, Ellis Mitrou, & Philip Wong

Date: 2018

Type: Article de revue / Article

Référence: Pham, Q.-V. V., Lavallee, A.-P., Foias, A., Roberge, D., Mitrou, E., & Wong, P. (2018). Radiotherapy immobilization mask molding through the use of 3D-printed head models. *Technology in Cancer Research & Treatment*, 17, 1533033818 (8 pages).
Citation: <https://doi.org/10.1177/1533033818809051>

Document en libre accès dans PolyPublie

Open Access document in PolyPublie

URL de PolyPublie: <https://publications.polymtl.ca/5085/>
PolyPublie URL:

Version: Version officielle de l'éditeur / Published version
Révisé par les pairs / Refereed

Conditions d'utilisation: Creative Commons Attribution-Utilisation non commerciale 4.0
Terms of Use: International / Creative Commons Attribution-NonCommercial 4.0
International (CC BY-NC)

Document publié chez l'éditeur officiel

Document issued by the official publisher


Titre de la revue: Technology in Cancer Research & Treatment (vol. 17)
Journal Title:

Maison d'édition: Sage Journals
Publisher:

URL officiel: <https://doi.org/10.1177/1533033818809051>
Official URL:

Mention légale:
Legal notice:

Radiotherapy Immobilization Mask Molding Through the Use of 3D-Printed Head Models

Technology in Cancer Research & Treatment
Volume 17: 1-8
© The Author(s) 2018
Article reuse guidelines:
sagepub.com/journals-permissions
DOI: 10.1177/1533033818809051
journals.sagepub.com/home/tct


Quoc-Viêt Vincent Pham¹ , Annie-Pier Lavallée, BEng²,
Alexandru Foias, CAPM, MScA³, David Roberge, MD, FRCPC^{4,5} ,
Ellis Mitrou, MSc⁴, and Philip Wong, MSc, MD, FRCPC^{4,5} 

Abstract

Purpose: To evaluate the feasibility of a workflow free of a simulation appointment using three-dimensional-printed heads and custom immobilization devices. **Materials and Methods:** Simulation computed tomography scans of 11 patients who received radiotherapy for brain tumors were used to create three-dimensional printable models of the patients' heads and neck rests. The models were three-dimensional-printed using fused deposition modeling and reassembled. Then, thermoplastic immobilization masks were molded onto them. These setups were then computed tomography-scanned and compared against the volumes from the original patient computed tomography-scans. Following translational \pm rotational coregistrations of the volumes from three-dimensional-printed models and the patients, the similarities and accuracies of the setups were evaluated using Dice similarity coefficients, Hausdorff distances, differences in centroid positions, and angular deviations. Potential dosimetric differences secondary to inaccuracies in the rotational positioning of patients were calculated. **Results:** Mean angular deviation of the 3D-printout from the original volume for the Pitch, Yaw, and Roll were 1.1° (standard deviation = 0.77°), 0.59° (standard deviation = 0.41°), and 0.79° (standard deviation = 0.86°), respectively. Following translational + rotational shifts, the mean Dice similarity coefficients of the three-dimensional-printed and original volumes was 0.985 (standard deviation = 0.002) while the mean Hausdorff distance was 0.9 mm (standard error of the mean: 0.1 mm). The mean centroid vector displacement was 0.5 mm (standard deviation: 0.3 mm). Compared to plans that were coregistered using translational + rotational shifts, the D_{95} of the brain from three-dimensional-printed heads adjusted for TR shifts only differed by -0.1% (standard deviation = 0.2%). **Conclusions:** Patient head volumes and positions at simulation computed tomography scans can be accurately reproduced using three-dimensional-printed models, which can be used to mold radiotherapy immobilization masks onto. This strategy, if applied on diagnostic computed tomography scans, may allow symptomatic and frail patients to avoid a computed tomography-simulation and mask molding session in preparation for palliative whole brain radiotherapy.

Keywords

brain, radiotherapy, 3D printing, simulation, palliative, immobilization

¹ Faculty of Medicine, University of Montreal, Montréal, Québec, Canada

² Département de génie de la production automatisée, École de technologie supérieure, Montréal, Québec, Canada

³ Department of Electrical Engineering, Institute of Biomedical Engineering, École Polytechnique Montréal, Montreal, Quebec, Canada

⁴ Department of Radiation Oncology, Centre Hospitalier de l'Université de Montréal, Montreal, Quebec, Canada

⁵ CRCHUM and Institut du Cancer de Montréal, Montreal, Quebec, Canada

Corresponding Author:

Philip Wong, MSc, MD, FRCPC, Department of Radiation Oncology, Centre Hospitalier de l'Université de Montréal, R10.466, 900 Rue St. Denis, Montreal, Quebec, Canada H2X 0A9.

Email: philip.wong.chum@ssss.gouv.qc.ca



Creative Commons Non Commercial CC BY-NC: This article is distributed under the terms of the Creative Commons Attribution-NonCommercial 4.0 License (<http://www.creativecommons.org/licenses/by-nc/4.0/>) which permits non-commercial use, reproduction and distribution of the work without further permission provided the original work is attributed as specified on the SAGE and Open Access pages (<https://us.sagepub.com/en-us/nam/open-access-at-sage>).

Abbreviations

3D, three-dimensional; ABS, acrylonitrile butadiene styrene; CT, computed tomography; DSC, dice similarity coefficients; HU, Hounsfield units; PLA, polylactic acid; PTV, planning target volume; ROT, rotational; SD, standard deviation; TR, translational; WBRT, Whole brain radiotherapy.

Received: February 20, 2018; Revised: September 05, 2018; Accepted: September 28, 2018.

Introduction

The lifetime risk of being diagnosed with cancer is 40% among people living in developed countries.¹ Twenty to forty percent of patients with cancer will develop brain metastases.² Many patients with brain metastases are elderly and frail due to comorbidities, disease progression, and/or toxicities from prior and ongoing treatments. Whole brain radiotherapy (WBRT) is used to reduce neurological symptoms (eg, convulsions, headache, weakness, and numbness) from brain metastases.³

Patients referred for WBRT have had a prior diagnostic computed tomography (CT)-scan. Despite a prior CT scan, all patients undergo another simulation CT-scan (CT-sim), in which patients will be placed in a reproducible position to prepare for radiation treatments. Patients also endure a molding session to create a personalized plastic mask that secures the patient's head in a fixed position during the CT-sim and radiation treatments. Alternate techniques to immobilize patients for WBRT, such as ones based on the use of strip tapes instead of thermoplastic masks, had previously been evaluated for claustrophobic patients.⁴

Novel applications of additive manufacturing (three-dimensional [3D]-printing) technology in radiotherapy have primarily been used to print brachytherapy applicators and bolus materials to improve radiation dose delivery.⁵ A prior study has shown the feasibility of 3D-printing heads (3D-Head) and masks using CT-sim images.⁶ However, the authors did not describe its practical utilization, radiation dosimetry, and implementation. With the widespread commercialization of 3D-printers, the cost of 3D-Head has now been reduced to approximately CAD100 (actual material and personnel cost from this study). This cost is expected to decrease as 3D-printer technology evolves, and will likely be considerably less than the cost of the CT-sim and molding session.

We hypothesize that patient positions at CT scans can be reproduced using 3D-printer products, which would reduce the need of a CT-sim and molding session. The uptake of 3D-printer methodologies could liberate resources from Radiation Oncology departments and improve the patient experience by reducing visits, interventions, and waiting times (Figure 1).

Material and Methods

Institutional ethics approval (CE 15.157) was obtained for a retrospective review of the clinical data and images obtained from patients who received brain radiotherapy (Table 1).

Image Segmentation

Digital imaging and communication in medicine (DICOM) images obtained from the CT-sim of 11 patients were exported from the local radiotherapy planning system (Eclipse, Varian Medical Systems, Inc, Palo Alto, California) to an open source program (3D-Slicer, <http://www.slicer.org>).⁷ Autosegmentations of the head and neck rest contours were obtained by selecting for voxels with Hounsfield units (HU) between −650.00 and 2976.00. Subsequently, in another 3D modeling program (CATIA, Dassault Systèmes, Vélizy-Villacoublay, France), the contoured structures were processed to (1) smooth the exterior contours, (2) isolate the head and neck rest from the other auto-segmented structures (couch table), and (3) remove the structures within the head.

Three-Dimensional Model Design

The process of design and fabrication of the 3D-Head and neck rests (3D-NRs) are shown in Figure 2. The 3D-NRs are printed separately as, in practice, patients would rest their heads on the 3D-NRs to reassume the position of the 3D-Heads. The 3D-Head and 3D-NRs interiors were 10% filled (Figure 2). Four matching pins and holes (1 cm diameter) were designed and added to the posterior aspect of the 3D-Heads and anterior aspect of the 3D-NRs, respectively (Figure 2). These pins and holes served to realign the 3D-Heads' positions on the 3D-NRs to ensure an accurate reproduction of the original rotational position. The contours were converted into 3D-printing compatible STL files.

Three-Dimensional-Printing

Three-dimensional-printing was done using the Big Builder Dual-Feed printer (Builder 3D Printers BV, Noordwijkerhout, the Netherlands), which utilized the fused deposition method from polylactic acid (PLA) filaments at 0.3-mm deposition thickness. The 3D-Heads were placed on their 3D-NRs (using the pin and hole system for alignment) on a flat table top to simulate a radiation therapy couch. Thermoplastic masks (Aquaplast RT, Orfit, Wijnegem, Belgium) that covered from the top of the 3D-Head to the chin were then molded onto the system as is standard practice for WBRT patients.

Image Registration

The thermoplastic mask immobilized 3D-printed heads were CT scanned. The CT images were then imported into Eclipse

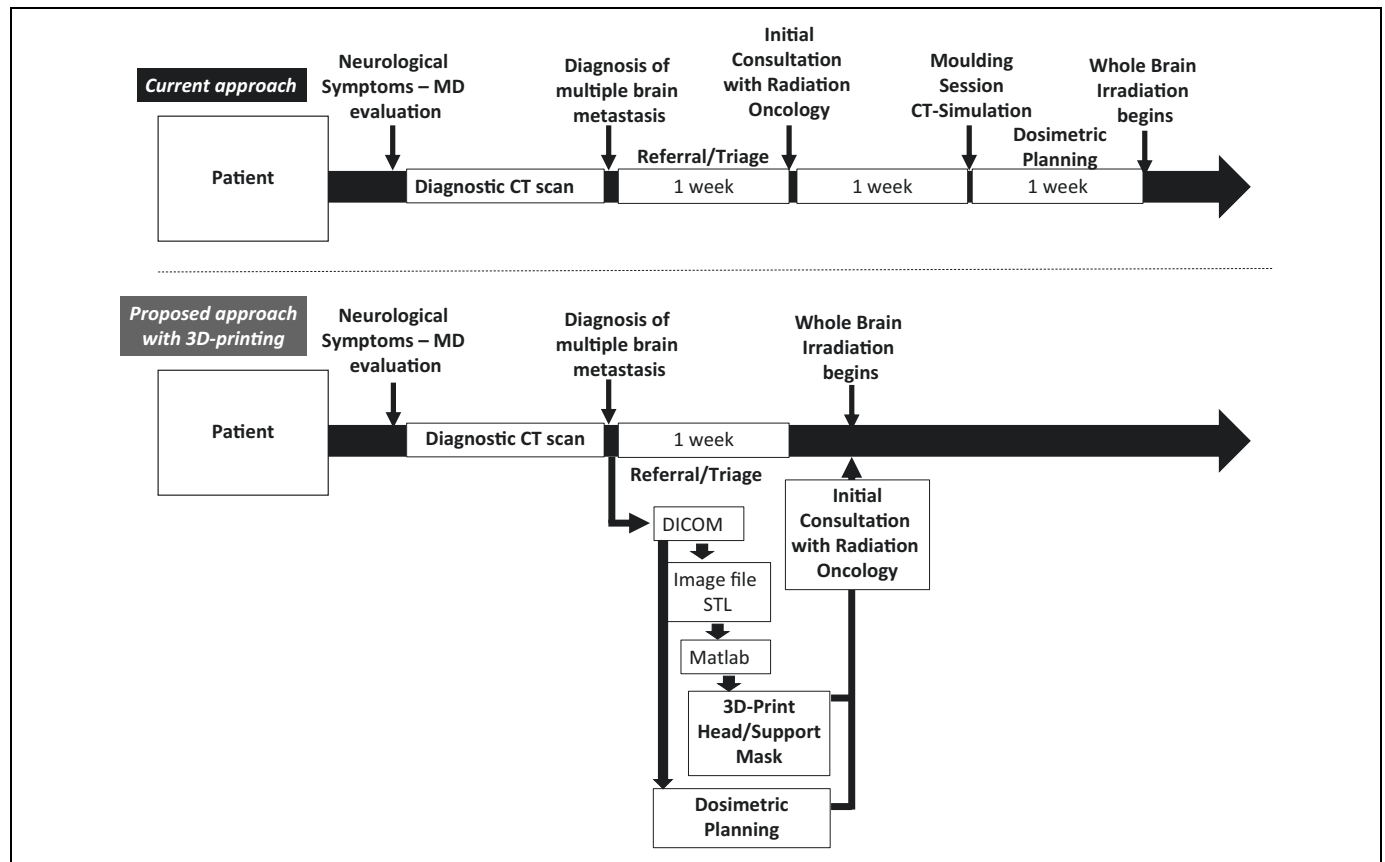


Figure 1. Current and proposed approaches for the elaboration of WBRT treatment. WBRT indicates whole brain radiotherapy.

Table 1. Characteristics of Patients and Structure Volumes.

Age	Gender	Tumor Histology	Head Volume (cc)	Brain Volume (cc)	Eyes Volume (cc)	3D-Head Volume (cc)	Head-3D-Head % Volume Difference
55	M	Meningioma	3558	1358	15	3522	−1.0
55	F	Endometrial cancer metastases	3429	1430	15	3384	−1.3
47	F	Lung cancer metastases	3256	1159	13	3153	−3.3
65	F	Endometrial cancer metastases	2713	1165	15	2698	−0.6
57	F	Breast cancer metastases	3422	1334	17	3331	−2.7
54	F	Lung cancer metastases	3838	1257	16	3798	−1.1
48	M	Kidney cancer metastases	3741	1421	13	3692	−1.3
85	F	Lung cancer metastases	3055	1149	13	3026	−0.9
71	F	Lung cancer metastases	3560	1412	14	3493	−1.9
52	F	Meningioma	4638	1597	25	4551	−1.9
69	F	Lung cancer metastases	4096	1375	14	4014	−2.0
Average (SD)			3573 (516)	1332 (139)	15 (3)	3515 (502)	−1.6 (0.8)

Abbreviations: 3D, three-dimensional; F, female; M, male; SD, standard deviation.

for image segmentation of the surface, to be compared with the original patient images (Figure 3).

Coregistrations of the images between the 3D-printed heads and the original patients were done using translational (TR) shifts on Eclipse or with the inclusion of rotational (TR + ROT) shifts using the iterative closest point method on 3D-Slicer. Following coregistration, the similarity between the 3D-Head and the original patient was measured using the Dice similarity index or coefficient (DSC):

$$DSC = \frac{2 * |A \cap B|}{|A| + |B|}$$

A is the total number of pixels that have intensity 1 in image A (also known as number of positives in A).

B is the total number of pixels that have intensity 1 in image B (also known as number of positives in B).

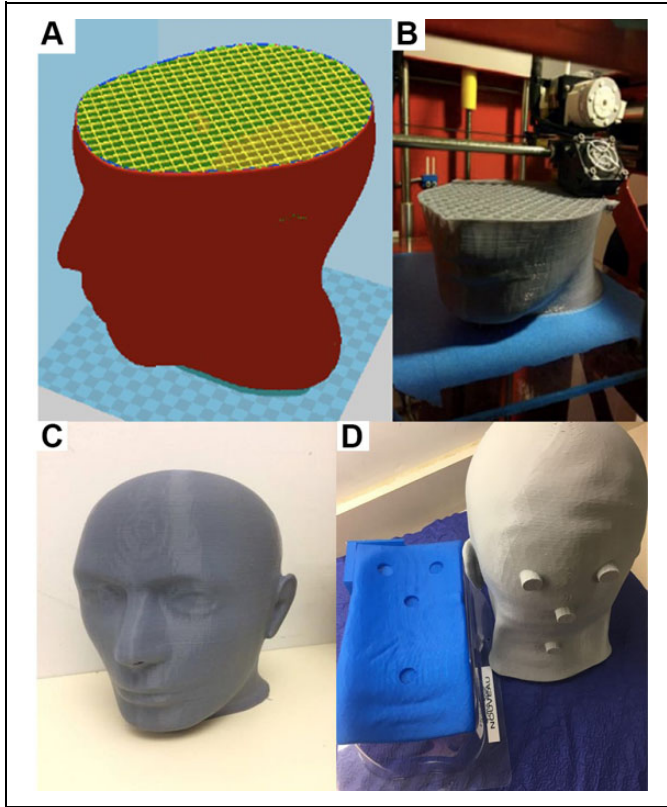


Figure 2. 3D-printing process. The printing time and amount of material used for 3D-printing was reduced by filling the head at 10% (A and B). The head (C) and neck rest were printed independently using polylactic acid filaments at 0.3 mm deposition thickness. Four pins and holes (D) were added to the head and neck rest to realign the 3D-printouts prior to thermoplastic masks molding. 3D indicates three-dimensional.

Pixels which have the value 1 in both *A* and *B* are known as *True Positives [TP]*.

The DSC ranges from 0 to 1, with values approaching 1 representing higher similarities between 2 objects.⁸

Accuracy was calculated using the following formula:

$$\text{Accuracy} = \frac{TP + TN}{TP + TN + FP + FN}$$

TN (True Negative) represents the total number of pixels, which have the value 0 in both *A* and *B*.

FP (False Positive) and *FN* (False Negative) represents the total number of pixels, which have discordant values between *A* and *B*.

The differences in the distances between the volumes were evaluated by collecting the maximum, mean, and 95% Hausdorff distances. The Hausdorff distance represents the maximum minimum Euclidean distance between the points of the 2 surfaces. Finally, the centroid locations of the volumes were calculated on a 3D-Slicer and compared.

A difference in the centroid location between the volumes ≤ 4 mm was determined a priori to be clinically acceptable as the institutional planning target volume (PTV) margin for WBRT

is 4 mm. A difference of $\leq 3^\circ$ in rotation was determined a priori to be clinically acceptable as this represents the maximum degree of rotational adjustment achievable using 6D radiotherapy couches.

Radiation Dosimetry

To evaluate the dosimetric consequence of not correcting for rotational differences, contours of patients' brain and eyes were copied onto the TR + ROT coregistered 3D-printed heads. Brain and eyes were contoured manually by a radiation oncologist (PW). Whole brain radiotherapy plans using 2 opposing lateral fields, usually with wedges, were planned on Eclipse. The plans were generated on the CT-sim scans of the original human heads with the multileaf collimator fields defined as the brain plus a margin of 8 mm. Dose was calculated with heterogeneity corrections turned off. The simulated prescription for WBRT was 30 Gy in 10 fractions. The WBRT plan was transposed onto TR or TR + ROT coregistered 3D-Heads. The HU values of the external contour of the 3D-Head images were set to zero and dose was calculated. The plans for the TR and TR + ROT coregistered CT sets were compared between each other to determine the potential effect of using translation shifts only for clinical matching before treatment.

Results

Dice Similarity Coefficients, Accuracy, and Volumes

After TR coregistration (no rotations), the mean DSC was 0.981 (standard deviation [SD]: 0.007) and the accuracy was 98.4% (SD: 0.69%). When rotational shifts were included in the coregistration (TR + ROT), the mean DSC improved to 0.985 (SD: 0.0030) and the accuracy was also improved to 98.8% (SD: 0.50%; Table 2; Figures 3 and 4). The 3D-Heads were on average 1.6% (SD: 0.8%) smaller than patient heads (Table 1). Overall, the similarity between the 3D-Heads and original head was high.

Hausdorff Distance

After TR shift only, the average maximum, average mean, and average 95% Hausdorff distances were 7.7 mm (SD: 1.7 mm), 1.3 mm (SD: 0.3 mm), and 4.1 mm (SD: 5.0 mm), respectively. After TR + ROT shifts, the average maximum, average mean, and average 95% Hausdorff distances were 7.4 mm (SD: 2.4 mm), 0.9 mm (SD: 0.1 mm), and 2.3 mm (SD: 0.6 mm), (Table 2) respectively. Thus, ROT adjustments further reduced the average 95% Hausdorff distances by 1.8 mm.

Centroid Displacement

Following coregistration using TR shifts only, the mean 3D distance between the centers of mass (centroid) of each volume was 1.6 mm (SD: 0.9 mm). After correcting for TR + ROT, the mean distance of the centroids was reduced to 0.5 mm (SD: 0.3 mm; Table 2).

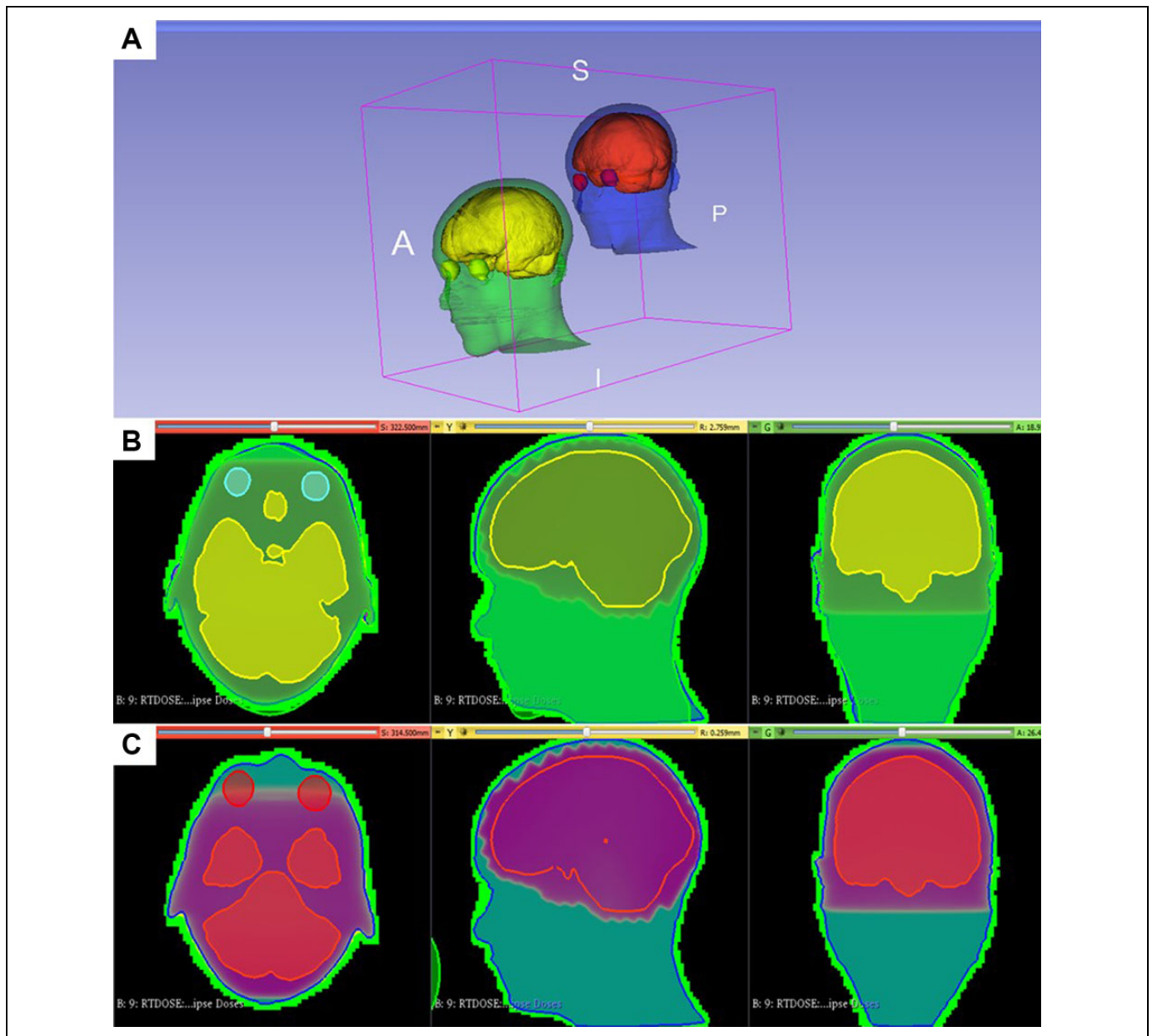


Figure 3. Coregistration images. The surface volume, brain, and eyes of the original images were coregistered with the images obtained from the 3D-printout using 3D Slicer. The colors and volumes of the 2 sets of images are displayed in (A): The human surface contour is in green and the 3D-printout surface contour is in blue. The human brain volume is in yellow and the 3D-printout brain is in orange. The human eyes are in cyan blue and the 3D-printout eyes are in red. Small discrepancies between the 2 surface volumes are distinguished as blue contours beyond the green contours (B). Following coregistration, the dosimetry from the human plan was applied onto the 3D-printout volumes (C) to quantify the dosimetric differences to the brain and eyes. 3D indicates three-dimensional.

Angles of Rotation

Table 2 describes the average Yaw, Pitch, and Roll angles of deviations from the original volume (after correcting for TR) were 0.59° (SD: 0.41°), 1.1° (SD: 0.77°), and 0.79° (SD: 0.86°), respectively. These rotational differences are within the institutional limits for WBRT (3°) and could be corrected with 6D couches.

Dosimetry

To determine the effect of correcting the patient's position only using translational table motion, the dose difference between the TR coregistered and TR + ROT coregistered 3D-printed plans was calculated. Table 3 describes the mean % dose differences of the D_{mean} , D_{95} , and D_{max} of the brain (target volume) were -0.06% (SD: 0.1%), 0.1% (SD: 0.2%), and -0.04%

Table 2. Coregistration Results.

Values of the Coregistration	Translational Coregistration	Translational + Rotational Coregistration
DSC, Mean (SD)	0.981 (0.007)	0.985 (0.002)
Accuracy, Mean (SD)	98.4% (0.7%)	98.8% (0.5%)
Centroid vector difference, Mean (SD)	1.6 mm (0.9 mm)	0.5 mm (0.3 mm)
Maximum Hausdorff distance, Mean (SD)	7.7 mm (1.7 mm)	7.4 mm (2.4 mm)
Average Hausdorff distance, Mean (SEM)	1.3 mm (0.3 mm)	0.9 mm (0.1 mm)
95% Hausdorff distance, Mean (SD)	4.1 mm (5.0 mm)	2.2 mm (0.6 mm)
Angle of deviation values (°)	Average	SD
Mediolateral or yaw angle	0.59	0.41
Anteroposterior or pitch angle	1.1	0.77
Longitudinal or roll angle	0.79	0.86

Abbreviations: DSC, dice similarity coefficients; SD, standard deviation; SEM, standard error of mean.

(SD: 0.1%). For the eyes, the mean % dose difference for the D_{\max} was -1.6% (SD: 3.0%). These dosimetric differences (1.8-45 cGy) are acceptable within the current clinical context.

Discussion

Our results suggest that a patient's head surface geometry can be accurately reproduced using 3D-printer technology. The positioning can be accurately reproduced using the 3D-Head and 3D-NR along with the pins and holes. These 3D impressions can then be used as a surrogate to mold radiotherapy thermoplastic immobilization masks for daily WBRT.

Prior studies evaluating the accuracy of auto-segmentation and coregistration algorithms for radiotherapy of the head and neck regions described a DSC of 0.5 to 0.95 for bone, which was often the most concordant structure.^{9,10} Using Hausdorff distances as a metric of coregistration accuracy, prior studies had observed mean Hausdorff distances to range from 2 to 5 mm.¹⁰⁻¹² The mean Hausdorff distance of this study (0.87-1.3 mm) was found to be well within this range. The largest discrepancies were found to be at the ears, where segmentation smoothing was applied. Nevertheless, the high DSC (mean:

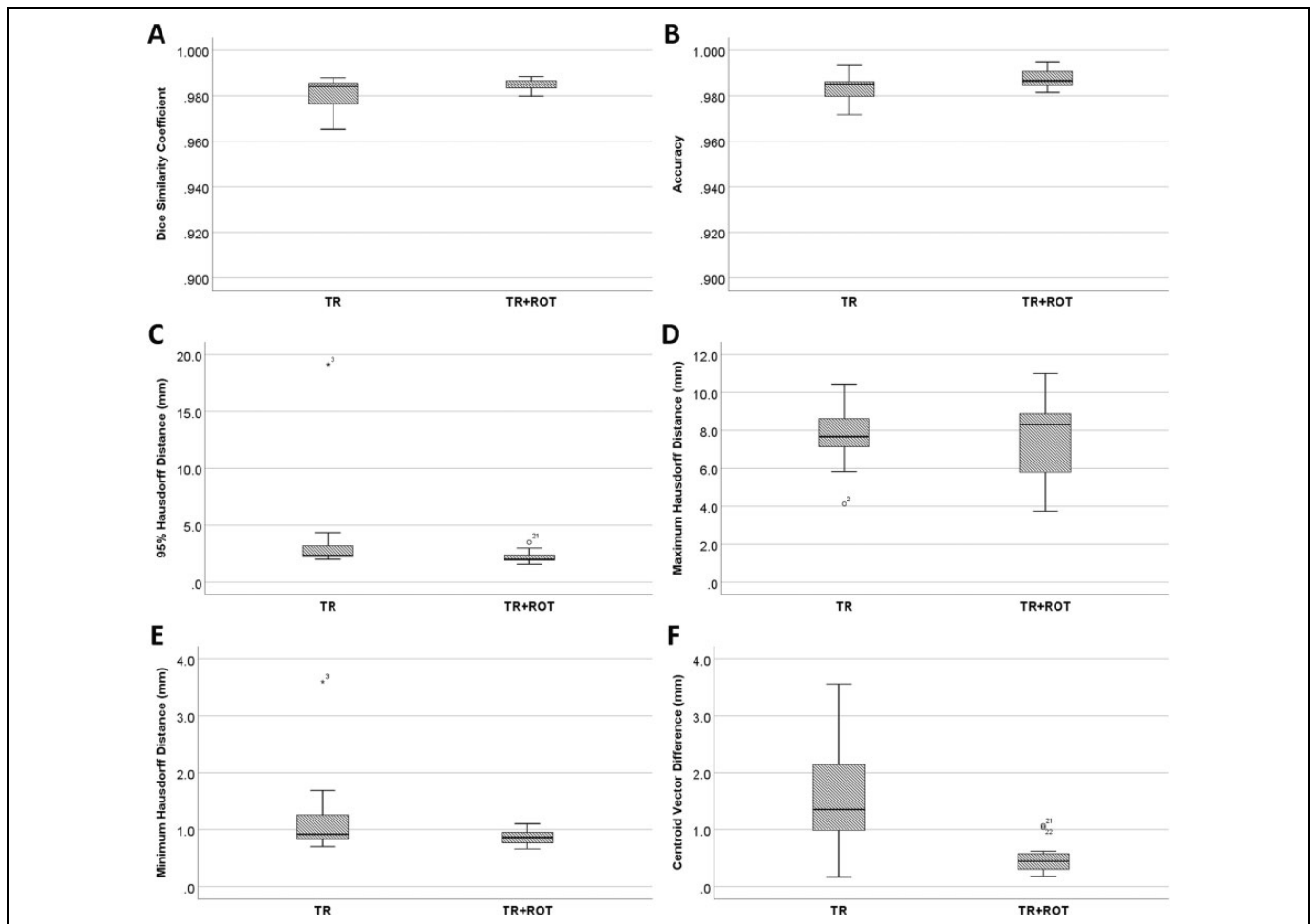


Figure 4. Coregistration comparisons. Following translational (TR) or translational + rotational (TR+ROT) coregistrations, (A) the dice similarity coefficient, (B) accuracy, (C-E) Hausdorff distances, and (F) centroid vector differences from the original head were calculated.

Table 3. Radiation Dose Differences to the Brain and Eyes if Rotational Shifts Were Not Applied.

		Brain Mean	Brain Min	Brain Max	Brain D95	Eyes Max
ROT+TR coregistered 3D printed plan	Avg (cGy)	3133	2792	3323	3018	3044
	SD (cGy)	214	215	234	214	275
Difference between 3D-printed plans registered using ROT+TR versus TR shifts		% Dose difference				
	Avg (%)	−0.06	−1	−0.04	−0.1	−1.6
	SD (%)	0.1	2	−0.1	0.2	3.0
		Dose difference				
	Avg (cGy)	−1.8	−30	−1.1	−3.1	−45
	SD (cGy)	2.7	43	4.0	5.3	85

Abbreviations: Avg, average; ROT, rotational; SD, standard deviation; TR, translational.

0.981) coefficients of this study demonstrated a good reproduction of the overall volume and position when using translational couch motion to correct for daily patient positioning. Given our institutional PTV margin of 4 mm in WBRT, the current strategy was deemed acceptable for further clinical evaluation in its capacity to replace CT-sim for WBRT patients.

Certain radiation therapy establishments have access to a radiotherapy treatment table that allows for rotational correction of the patient's position (6D couches). We explored the applicability of our strategy if rotational shifts were employed. Our results indicated that the incorporation of rotational adjustments increased the mean DSC from 0.981 to 0.985 and reduced the mean centroid displacement from 1.6 mm to 0.5 mm. The accuracy of the proposed strategy was within the institutional constraints (≤ 4 mm, $\leq 3^\circ$) for clinical use in WBRT.

The proposed workflow implies planning on a diagnostic CT image set and delivering said treatment plan on the patient using a thermoplastic mask that was derived from the 3D impression of the patient. Assuming that daily image guidance is used to reposition patients using TR shifts, the main dosimetric impact of this workflow distills down to the exactitude of patient rotational positioning pretreatment within the thermoplastic mask. Without 6D couch correction, this means comparing the dose difference on a structure set that was registered using TR shifts only to that of a structure set that was registered using both TR + ROT shifts. Given that we are using parallel opposed fields, the differences are expected to be small, as is the case for the brain target structure, with an average D₉₅ dose difference of 0.1%. For the eyes, since they are smaller structures, rotational displacements could result in important amounts of the structure to be included or excluded from the treatment fields. Therefore, the impact of ROT shifts to the dose received by the eyes is larger than for the brain. As expected, the average D_{max} received by the eyes differed by 1.6% or 45 cGy, which was still deemed a clinically acceptable difference.

Three-dimensional-printing technology is evolving rapidly along with reductions in costs, improvement in speed and

resolution, and an expanding array of printable materials. Prior studies conducted in 2014 determined that 3D printing of heads and masks for radiotherapy was feasible.⁶ Through the current study, we confirm that 3D printing of patient's head is indeed feasible with volumetric accuracy that is suitable for further clinical evaluation. Additionally, we printed 3D-NR with pins and holes to enhance our ability to reproduce a patient's CT scan position accurately using 3D-printed products.

In choosing the material for 3D-printing, PLA filaments were selected over acrylonitrile butadiene styrene (ABS) because (1) PLA is biodegradable and (2) upon cooling, PLA contracts less than ABS and therefore confers better geometric precision to 3D-printed products. Furthermore, PLA is common and affordable which rendered the material cost of our 3D-printing strategy for a set of 3D-Head and 3D-NR to be CAD30. Although we did not perform a formal cost analysis on the strategy, the cost of 3D-Head and 3D-NR is comparatively cheaper than that of a diagnostic or simulation CT scan (CAD200-400) at our institution, without considering the salary of the personnel operating the CT scan. The avoidance of an appointment to department could further reduce the cost (time and money) for the patient and his/her caregiver. Finally, the adoption of this strategy for WBRT would alleviate CT-sim time slots which could be used by other patients, thereby reducing the overall patient waiting time within the department.

There are several limitations to the current strategy and evaluation methodologies. First, the present method had only been tested in patients in standard head position using CT images obtained at the time of simulation. However, at the time of diagnostic CT scan, symptomatic patients with brain metastases might assume unconventional head positions, which could render the patient's head positioning less reproducible for daily WBRT. For example, a patient could have turned his/her head sideways or assumed a neck position that would limit the immobilization capability of thermoplastic masks or become too uncomfortable to be maintained during WBRT. As patients with brain metastases are often given corticosteroids, the surface volume of the patients could increase from the time of diagnostic CT scan due to steroid

induced water retention. Thus, the thermoplastic masks molded based on diagnostic CT scan images might become tight along with slight dosimetric differences. A potential solution to improve the mask's comfort level would be by expanding the patient's surface volume by 1 mm prior to 3D-printing. Also, thermoplastic masks may not be suitable for claustrophobic patients, for which other immobilization strategies may be needed.⁴ Finally, the current technique requires 36 hours to print the 3D-Head and 3D-NR for each patient. Therefore, this methodology would not be suitable for patients requiring WBRT within 1 to 2 days. Furthermore, as our institution treated approximately 200 patients annually with WBRT, at least 2 working 3D-printers would be needed to continuously generate 3D-printouts for this population.

Conclusions

Our study suggested that the reproduction of a patient's head volume and position using 3D-printing is feasible. The similarity and accuracy were sufficiently robust to yield minimal differences in the dosimetry of patients receiving WBRT. This strategy could reduce the need for simulation, thereby streamlining and simplifying the care pathways for patients with brain metastases.

Authors' Note

Quoc-Viêt Vincent Pham and Annie-Pier Lavallée, BEng, contributed equally. Ellis Mitrou, MSc and Philip Wong, MSc, MD, FRCPC contributed equally.

Acknowledgment

Authors thank Dr Julien Cohen-Adad in allowing our team to use his laboratory's 3D printer for this project.

Declaration of Conflicting Interests

The author(s) declared no potential conflicts of interest with respect to the research, authorship, and/or publication of this article.

Funding

The author(s) disclosed receipt of the following financial support for the research, authorship, and/or publication of this article: This work was supported by funds from the Institut de Cancer de Montréal and the University of Montreal Department of Radiology, Radiation Oncology and Nuclear Medicine Support Professoral.

ORCID iD

Quoc-Viêt Vincent Pham  <http://orcid.org/0000-0003-3383-2316>
David Roberge, MD, FRCPC  <http://orcid.org/0000-0001-8747-648X>
Philip Wong, MSc, MD, FRCPC  <http://orcid.org/0000-0002-7761-0283>

References

1. Canadian Cancer Statistics Advisory Committee. *Canadian Cancer Statistics 2018*. Toronto, Canada: Canadian Cancer Society. 2018. cancer.ca/Canadian-Cancer-Statistics-2018-EN. Accessed October 19, 2018.
2. Landis SH, Murray T, Bolden S, Wingo PA. Cancer statistics, 1999. *CA Cancer J Clin*. 1999;49(1):8-31.
3. McTyre E, Scott J, Chinnaiyan P. Whole brain radiotherapy for brain metastasis. *Surg Neurol Int*. 2013;4(suppl 4):S236-S244.
4. Rubinstein AE, Ingram WS, Anderson BM, et al. Cost-effective immobilization for whole brain radiation therapy. *J Appl Clin Med Phys Amer Coll Med Phys*. 2017;18(4):116-122.
5. Kim SW, Shin HJ, Kay CS, Son SH. A customized bolus produced using a 3-dimensional printer for radiotherapy. *PLoS One*. 2014;9(10):e110746.
6. Laycock SD, Hulse M, Scrase CD, et al. Towards the production of radiotherapy treatment shells on 3D printers using data derived from DICOM CT and MRI: preclinical feasibility studies. *J Radiotherapy Pract*. 2014;14(1):92-98.
7. Fedorov A, Beichel R, Kalpathy-Cramer J, et al. 3D slicer as an image computing platform for the quantitative imaging network. *Magn Reson Imaging*. 2012;30(9):1323-1341.
8. Dice LR. Measures of the amount of ecologic association between species. *Ecology*. 1945;26(3):297-302.
9. Edmund JM, Nyholm T. A review of substitute CT generation for MRI-only radiation therapy. *Radiat Oncol*. 2017;12(1):28.
10. Mohamed AS, Ruangskul MN, Awan MJ, et al. Quality assurance assessment of diagnostic and radiation therapy-simulation CT image registration for head and neck radiation therapy: anatomic region of interest-based comparison of rigid and deformable algorithms. *Radiology*. 2015;274(3):752-763.
11. Fisher M, Applegate C, Ryallat M, et al. Evaluation of 3-D printed immobilisation shells for head and neck IMRT. *Open J Radiol*. 2014;4:322-328.
12. Ghose S, Holloway L, Lim K, et al. A review of segmentation and deformable registration methods applied to adaptive cervical cancer radiation therapy treatment planning. *Artif Intell Med*. 2015; 64(2):75-87.